Supplement of Solid Earth, 9, 649–668, 2018
https://doi.org/10.5194/se-9-649-2018-supplement

Solid Earth Open Access EGU

Supplement of

Effects of upper mantle heterogeneities on the lithospheric stress field and dynamic topography

Anthony Osei Tutu et al.

Correspondence to: Anthony Osei Tutu (oseitutu@gfz-potsdam.de)

Contents

Introduction

The main text shows the model input and results from our series of calculations with the lithosphere-asthenosphere code coupled to the mantle flow code to evaluate the influence of the mantle flow and lithosphere density anomalies on lithosphere stress and topography. Here we show additional figures of model input and results which did not go into the main text but are referred to in the main text, e.g. modeled stress and topography with other upper mantle thermal structures. In this current study:

1. We evaluate the influence of shallow and deep Earth thermal-and-density heterogeneities on global lithospheric stress field and dynamic topography.

2. We compare the modeled stress field to the World Stress Map 2016 and the corresponding dynamic topography to two independent observation-based residual topography models.

3. Upper mantle thermal structures inferred from the S-wave velocity model fit the observed topography much better when continental depletion are corrected for, but there is almost no improvement in the respective stress field.

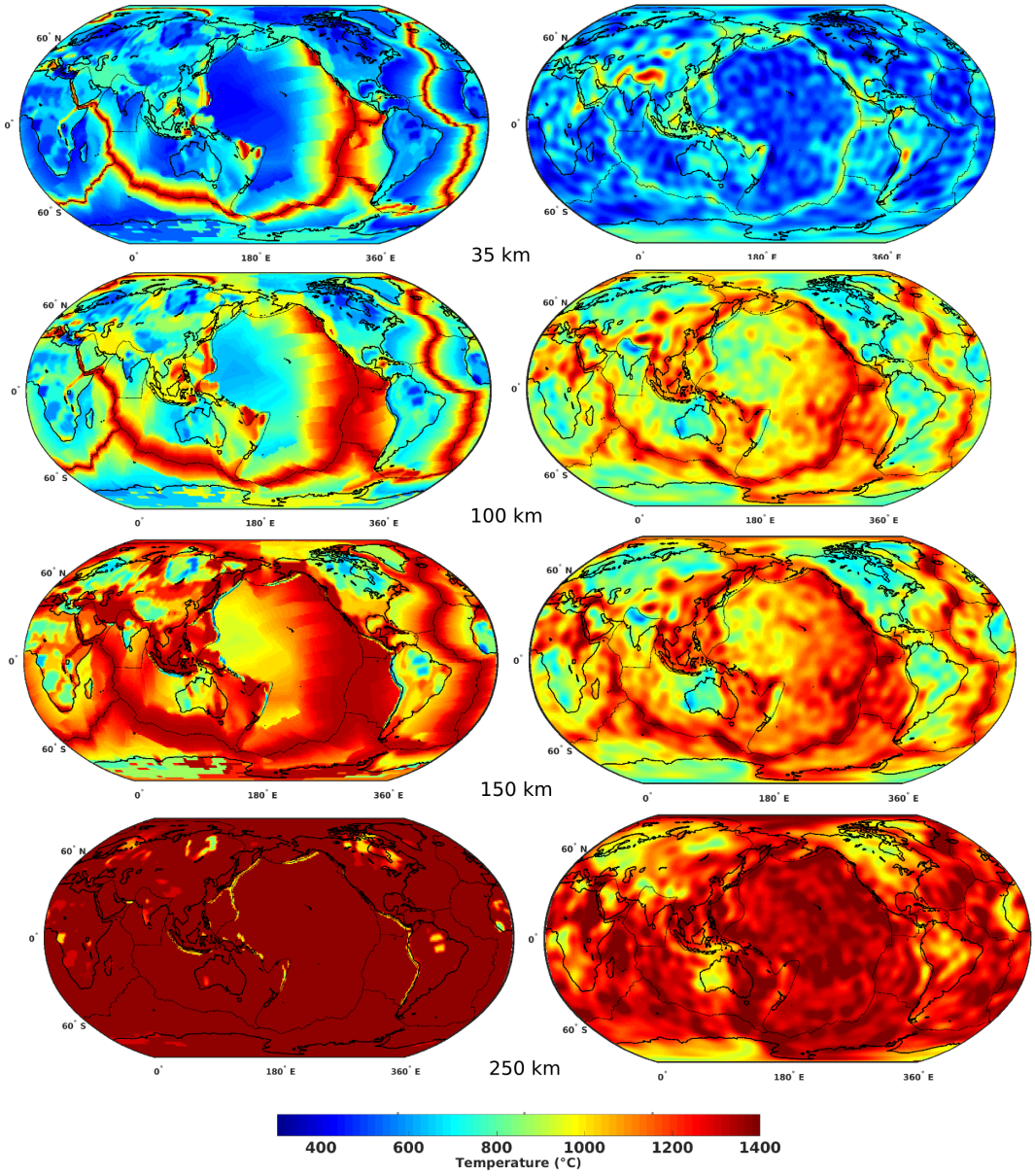

Figure S1. The thermal structure of the upper mantle at a depths of 35, 100, 150, and 250 km from the two reference thermal models adopted in this study, TM1 (left column) and TM2 (right column). TM1 is derived from the thermal structure TC1 of Artemieva (2006) in the continents and the sea floor age model of Müller et al. (2008) in the oceanic areas, while the TM2 model is based on the S-wave tomography-model SL2013sv from Schaeffer and Lebedev (2013) for inferring thermal structure in the upper 300 km. We explicitly account for slabs in the TM1 as shown in slices at 150 and 250 km.

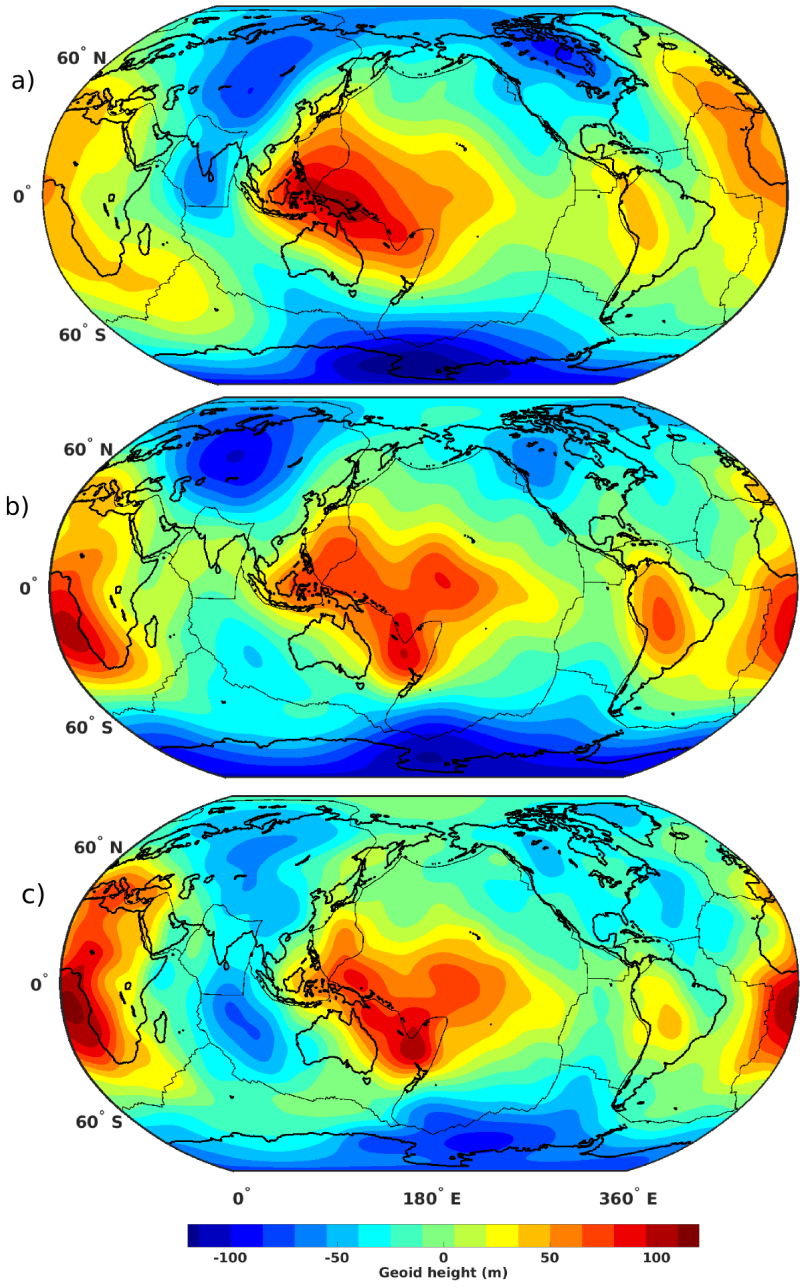

Figure S2. Comparing (a) the observed geoid from GRACE (with the effect of hydrostatic equilibrium removed) to our modeled geoid (b) using LVVs in the upper 300 km with only radial viscosity variation below and (c) with only radial viscosity variation (Steinberger and Calderwood, 2006) for all depths. The modeled geoid is estimated with the density distribution from Becker and Boschi (2002) below 300 km and TM1 thermal density structure in the top 300 km.

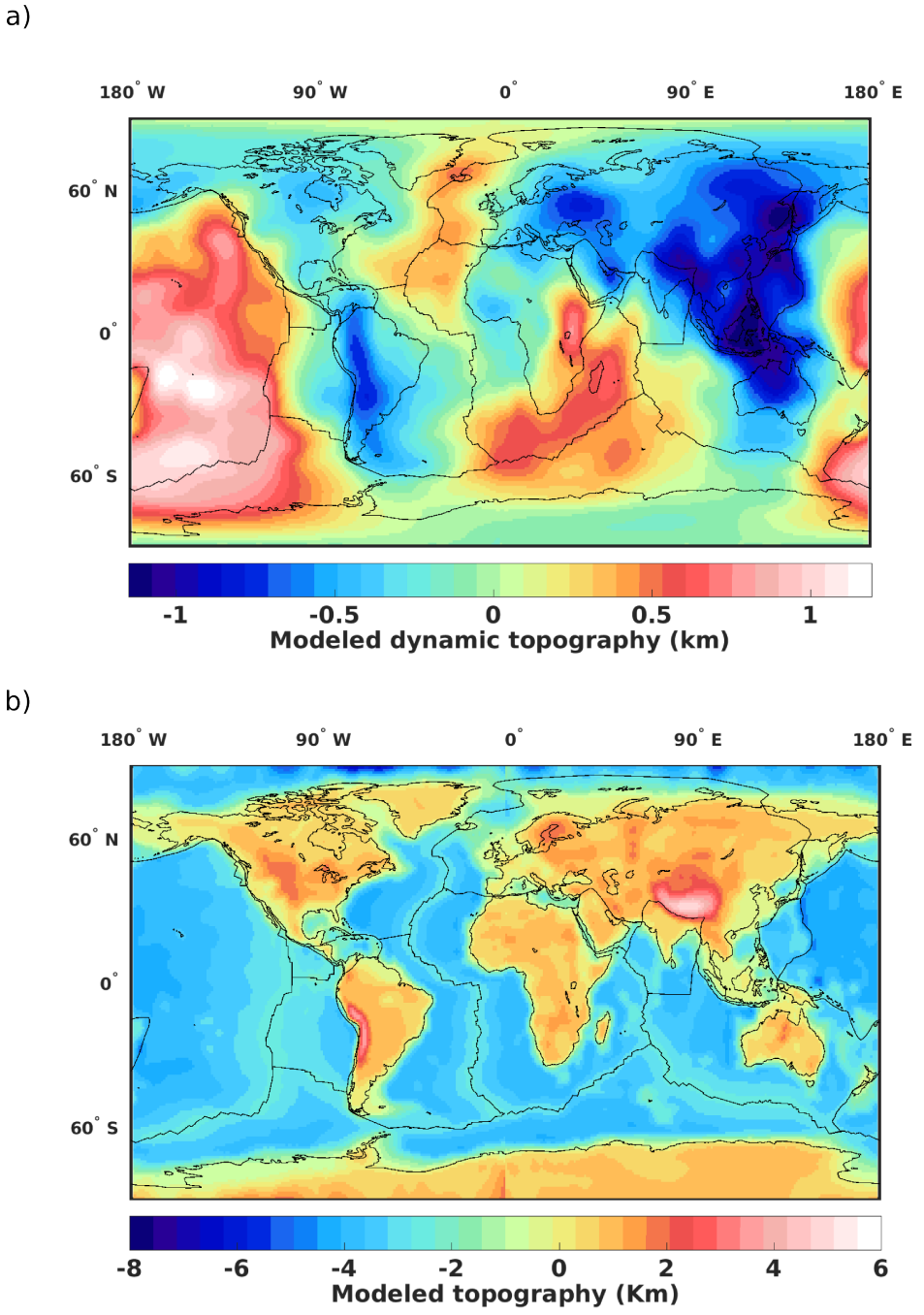

Figure S3. Model-based topography beneath air (free surface) (a) originating from mantle flow driven by density anomalies below 300 km (b) caused by structure of the top 300 km of the upper mantle, computed with the CRUST 1.0 model and TM1.

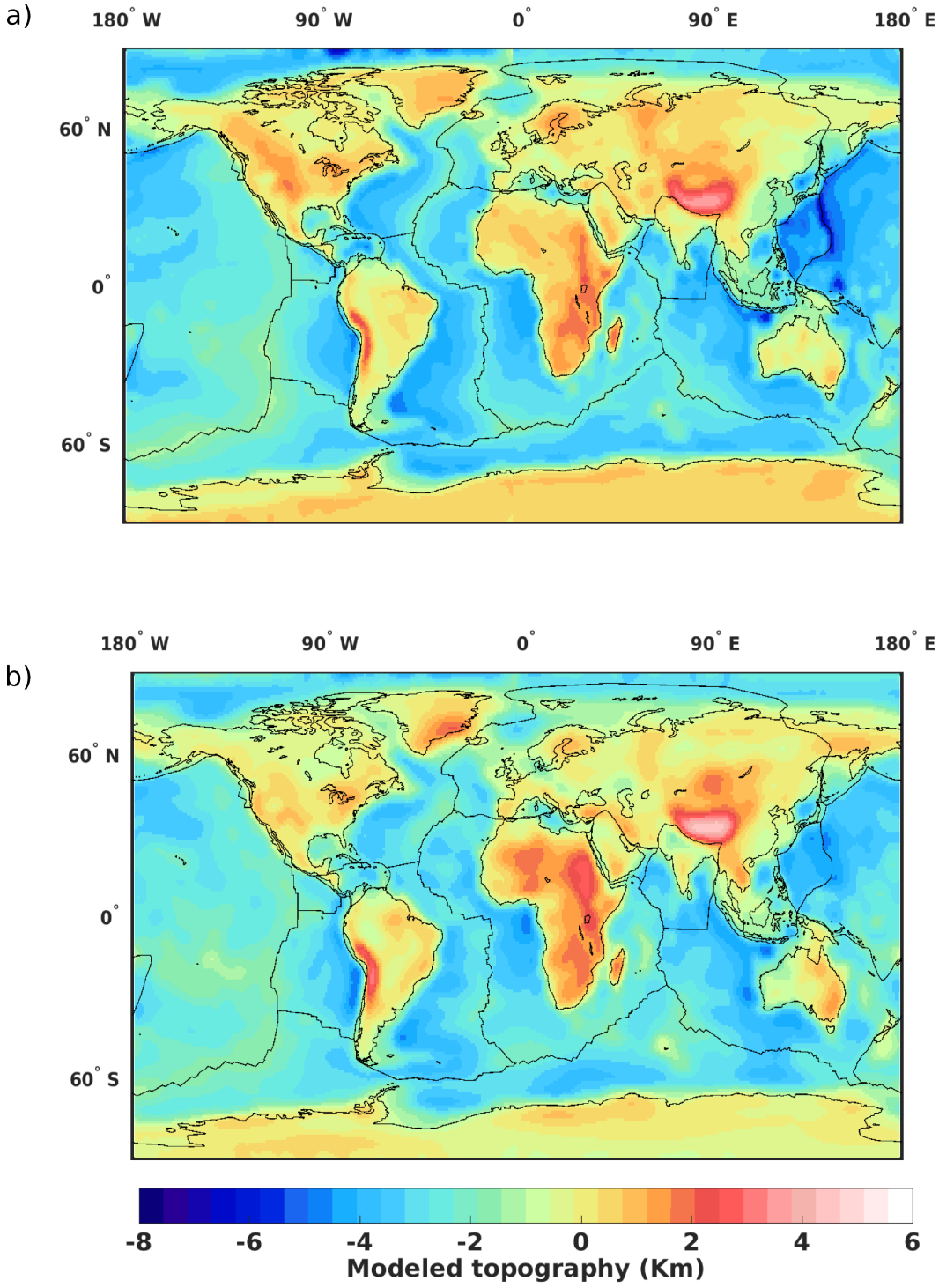

Figure S4. Predictions of the topography under air from combined contributions due to lower mantle flow and upper mantle from a) TM1 with crust model and b) TM2 with crust model.

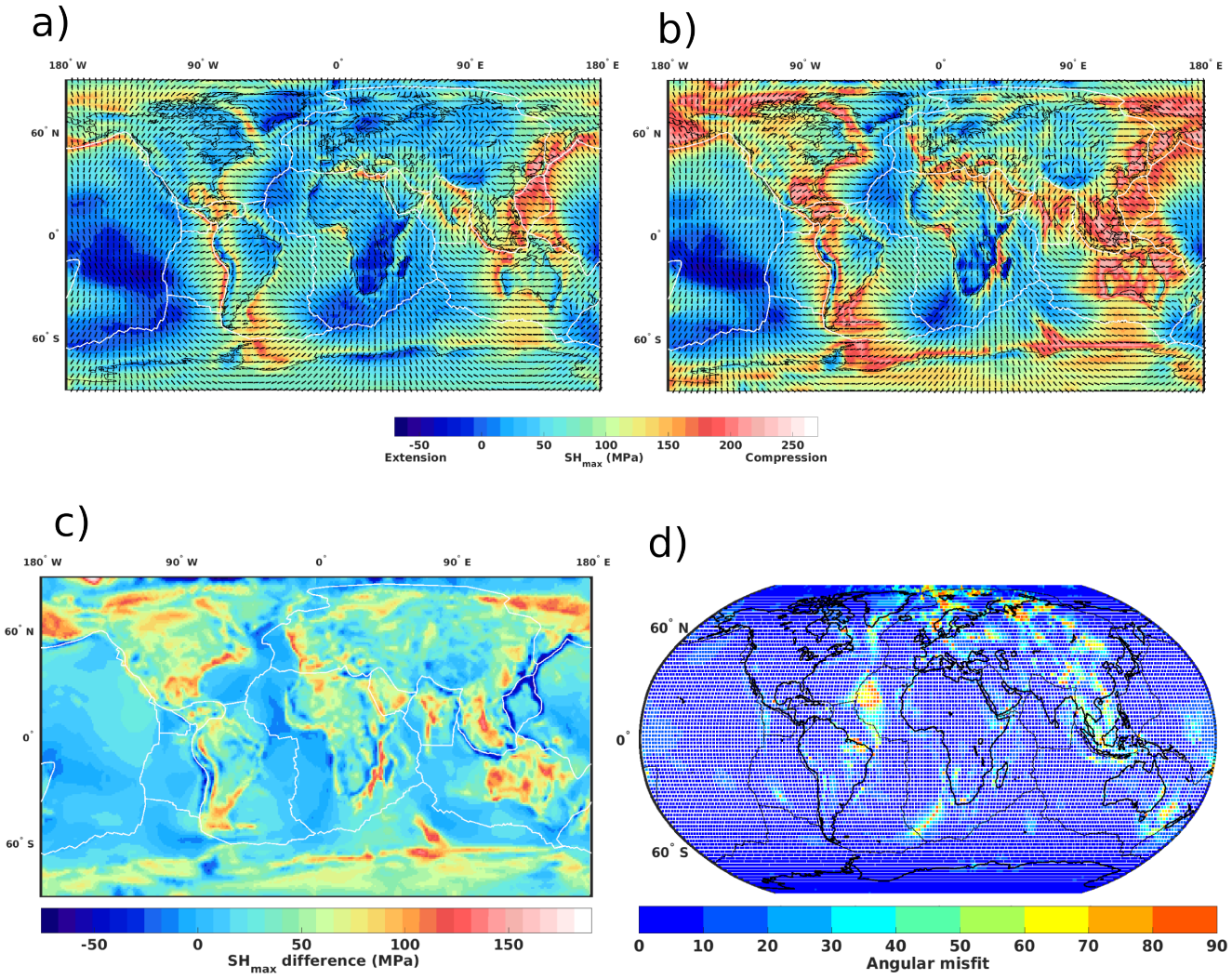

Figure S5. Predictions of the SH_{max} magnitude and direction from total contributions due to lower mantle flow and upper mantle thernal-density structure TM1 with CRUST 1.0 model a) considering elasticity and b) without elasticity. The resulting difference for c) stress magnitude and d) direction between scenario (a) and (b).

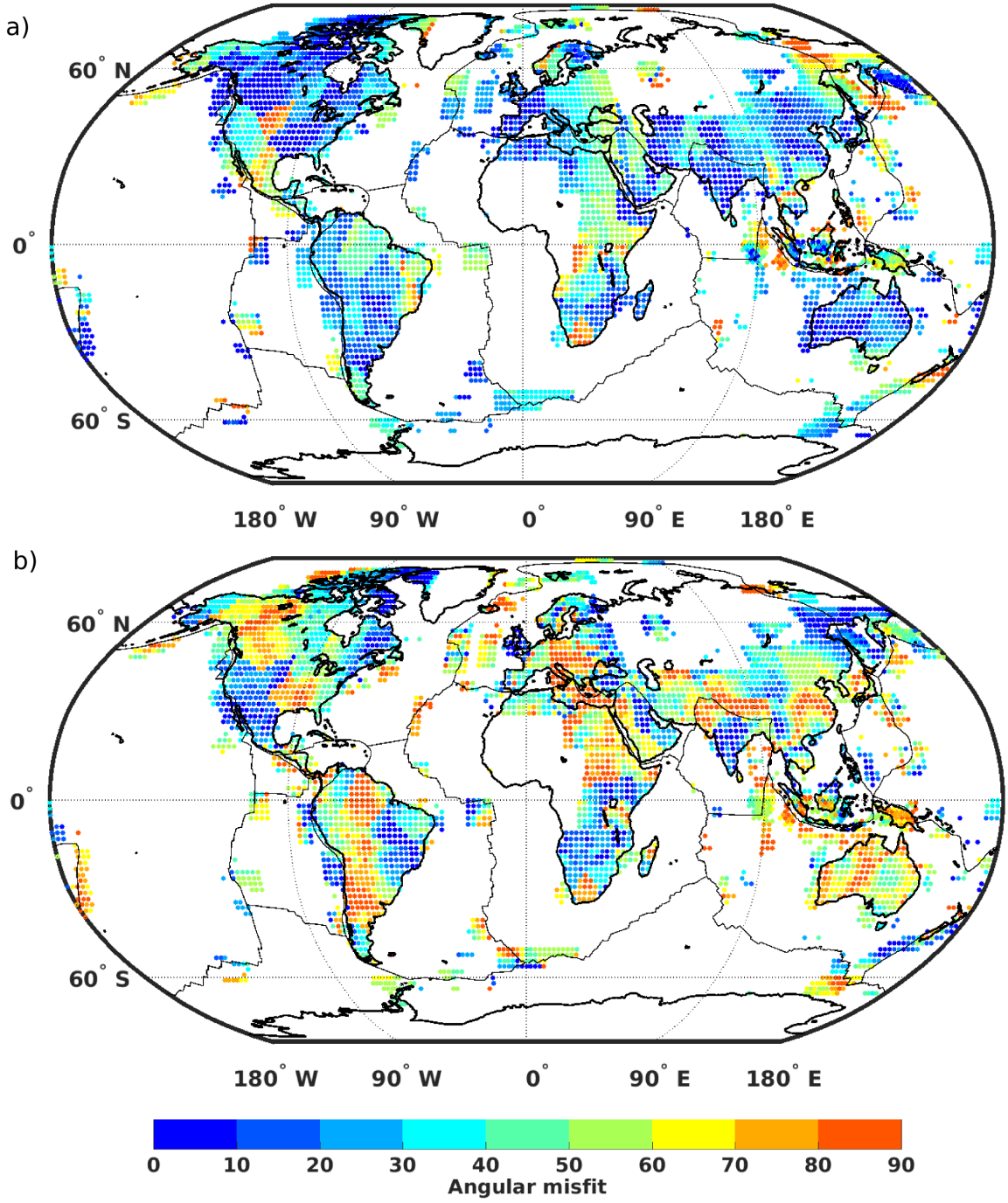

Figure S6. Angular misfit between the observed (WSM 2016) and modeled stress directions from (a) stress field originating from mantle flow driven by density anomalies below 300 km and (b) stress field from structure of the top 300 km of the upper mantle, computed with the CRUST 1.0 model and TM1.

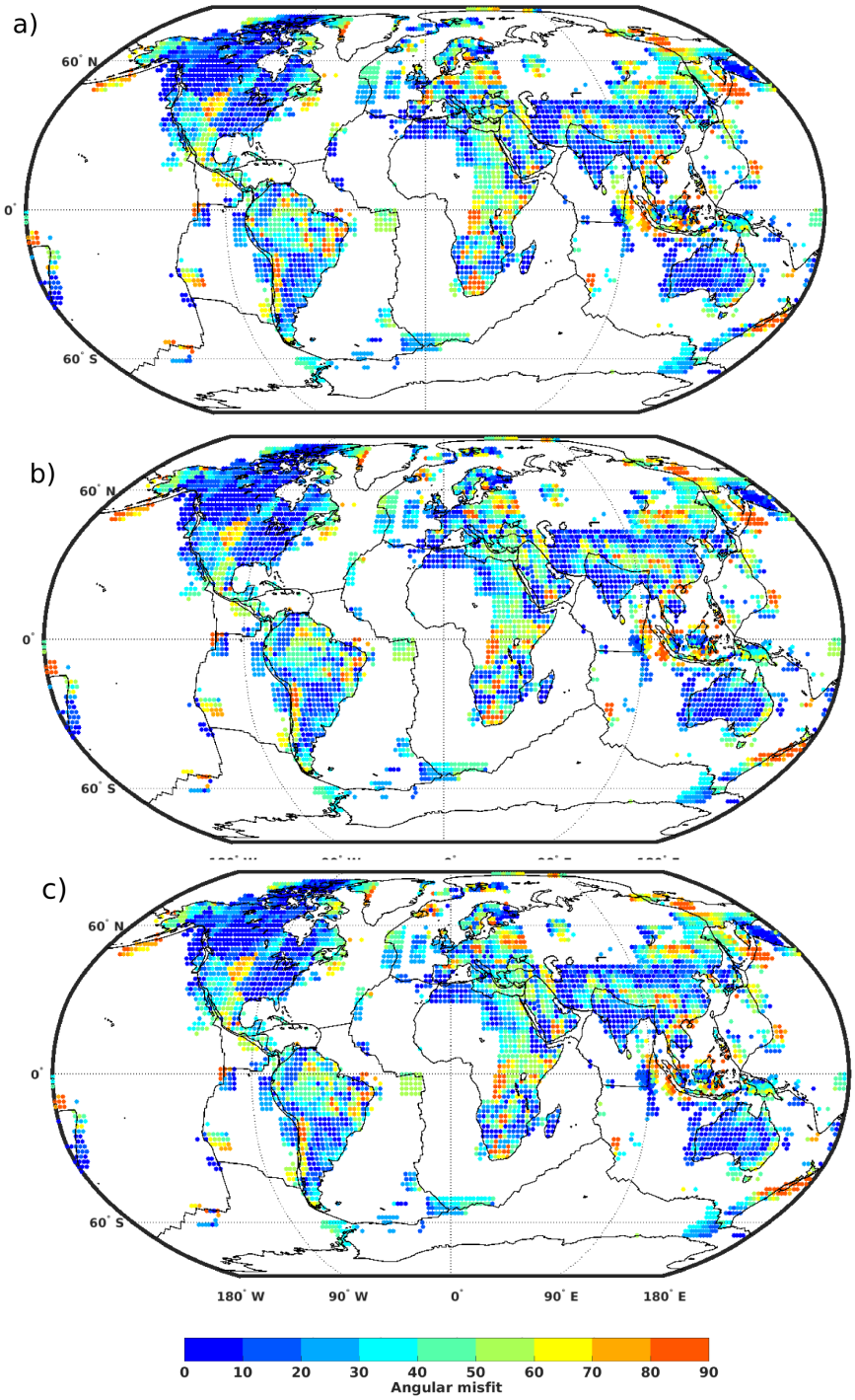

Figure S7. Angular misfit between the observed (WSM 2016) and total modelled stress direction with (a) TM2 with cratonic regions having added constant temperature of 300 K and (b) SAW24B16 with realistic treatment of craton using PerpleX after Cammarano et al. (2011) and (c) same with S20RTS for the upper mantle thermal and density structures.

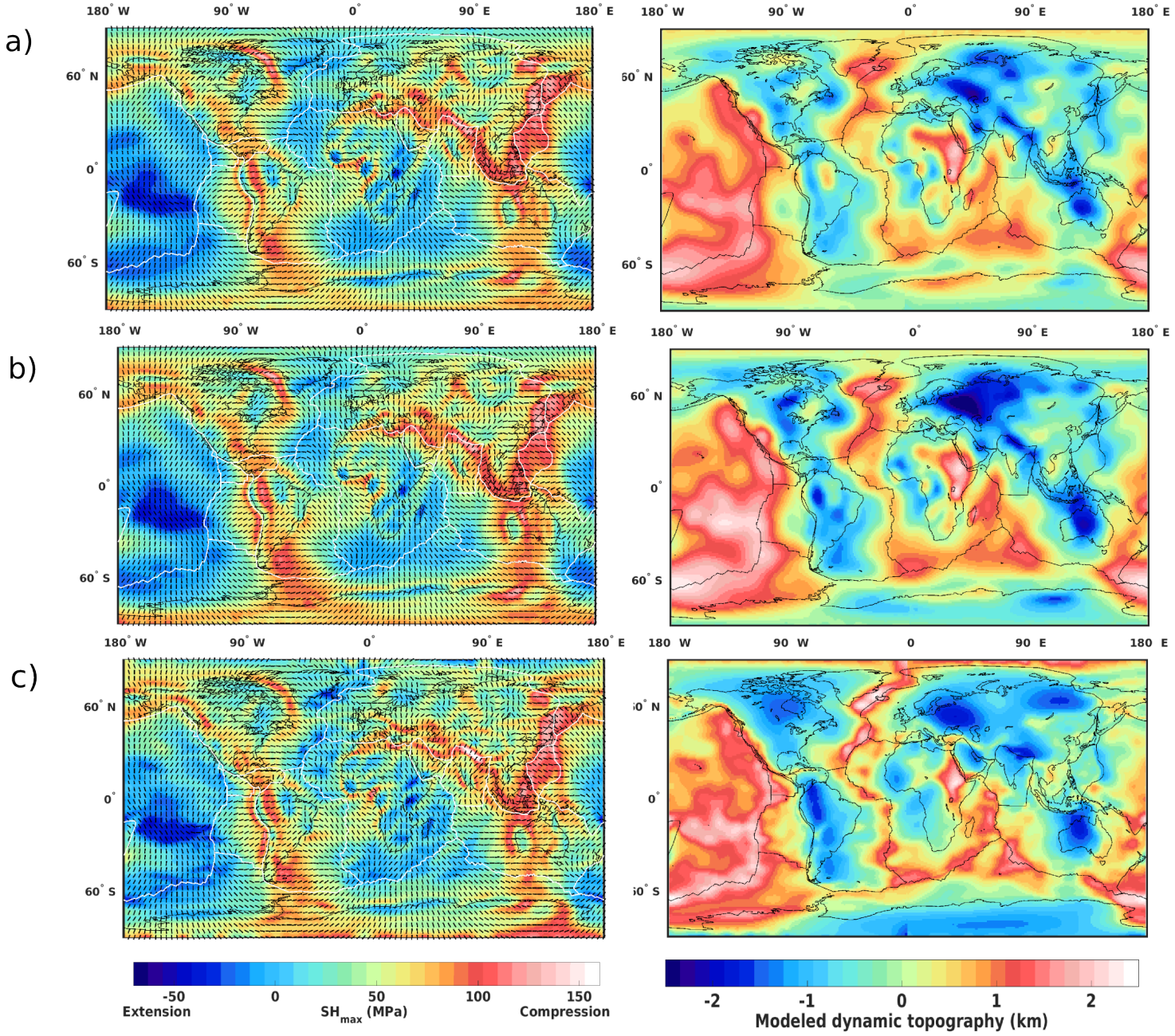

Figure S8. (left column) modeled lithospheric stress field without the effect of crustal thickness variations and (right column) corresponding dynamic topography for (a) TM2 (300 K additional temperature converted to density in crations to account for chemical deplection), (b) SAW24B16 with realistic treatment of cratons using PerpleX after Cammarano et al. (2011) and (c) same with S20RTS for the upper mantle thermal and density structures.

References

Artemieva, I.: Global $1^\circ \times 1^\circ$ thermal model $TC1$ for the continental lithosphere: implications for lithosphere secular evolution, Tectonophys., 416, 245–277, 2006.

Becker, T. W. and Boschi, L.: A comparison of tomographic and geodynamic mantle models, Geochem., Geophys., Geosys., 3, 1003, https://doi.org/10.1029/2001GC000168, 2002.

Cammarano, F., Tackley, P., and Boschi, L.: Seismic, petrological and geodynamical constraints on thermal and compositional structure of the upper mantle: global thermo-chemical models, Geophys. J. Int., 187, 1301–1318, 2011.

Müller, R. D., Sdrolias, M., Gaina, C., and Roest, W. R.: Age, spreading rates and spreading asymmetry of the world's ocean crust, Geochem., Geophys., Geosys., 9, Q04006, https://doi.org/10.1029/2007GC001743, 2008.

Schaeffer, A. and Lebedev, S.: Global shear speed structure of the upper mantle and transition zone, Geophys. J. Int., 194, 417–449, 2013.

Steinberger, B. and Calderwood, A.: Models of large-scale viscous flow in the Earth's mantle with constraints from mineral physics and surface observations, Geophys. J. Int., 167, 1461–1481, 2006.